Asian and Pacific Coasts 2005
September 4-8, 2005, Jeju, Korea

TURBULENT CHARACTERISTICS OF THE ATMOSPHERIC SURFACE LAYER IN THE INTER-TIDAL ZONE OF THE ARIAKE SEA

Kenji Tanaka[1], Akira Narimatsu[2], Kentaro Morimoto[3] and Kiyoshi Takikawa[4]

ABSTRACT: The characteristics of atmospheric turbulence over a large inter-tidal zone are investigated on the basis of atmospheric boundary layer observations. Turbulence in the atmospheric surface layer controls the energy interaction between the sea surface and the atmosphere, and thus plays an important role in the formation of the current field and the circulation of subsidence in sea regions. It is found that the Monin-Obukhov similarity theory is applicable to wind speed in the inter-tidal zone despite the heterogeneous and non-stationary surface characteristics. The nondimensional standard deviation of temperature and specific humidity also obey similarity theory under sea breeze conditions.

Keywords: inter-tidal zone, closed bay, atmospheric boundary layer, similarity theory, non-stationary surface

1. Introduction

The Ariake Sea is a typical closed bay on the west coast of Kyushu Island, Japan. The Ariake Sea has a dynamic tidal range, reaching more than 5 m in the closed-off section of the bay at the spring tide. The region also hosts a vast tidal flat that exposes an area of larger than 200 km^2 at the spring tide, representing about 40% of the total exposed tidal area of Japan. Several of the exposed coastal regions in the Ariake Sea extend for more than 1–2 km offshore depending on the tidal fluctuation.

The atmospheric turbulence over this inter-tidal zone has been thought to play an important role in driving the current (or wave) field and the circulation of subsidence accompanying the seawater current in sea regions. Many observational and numerical studies have been conducted in recent years on the atmospheric boundary layer in many areas including coastal regions (e.g., Plant et al., 2003; Kruit et al., 2004; Lange et al, 2004). However, although the growth of the internal boundary layer due to sea breeze circulation has been clarified to a considerable extent, the role of the variable land and sea surface of inter-tidal zones remains unclear.

The objective of the present study is to observe the turbulent characteristics of the atmospheric

[1]Research Associate, Department of Architecture and Civil Engineering, Kumamoto University, Kumamoto 860-8555, Japan. ktanaka@gpo.kumamoto-u.ac.jp
[2]Kyushu Regional Developed Bureau, Ministry of Land Infrastructure and Transport, Japan.
[3]Graduate School of Science and Technology, Kumamoto University, Kumamoto, 860-8555, Japan. morik en@gpo.kumamoto-u.ac.jp
[4]Professor, Center for Marine Environment Study, Kumamoto University, Kumamoto 860-8555, Japan. takikawa@gpo.kumamoto-u.ac.jp

boundary layer over the inter-tidal zone of the Ariake Sea. The applicability of the Monin-Obukhov similarity theory, which is defined for homogeneous steady surfaces, is also investigated.

2. Field Observation and site characteristics

The interaction of the land and sea surface with the atmosphere was observed using an automated weather station (AWS; Photo 1) deployed in the inter-tidal zone near Kumamoto Port (Fig. 1). The site is located approximately 600 m to the west of the Kumamoto Plane shoreline and 200 m north of Kumamoto Port (Yumesaki Island) (32°46'5" N, 130°35'40" E). The mouth of the Shira River is located approximately 1.0 km northeast of the AWS. In this region, the surface is exposed to about 1.5 km offsh[illegible]west water level. In the immediate vicinity of the observation site, the surface is exposed for up to 3.5 h at the peak of every half-day tidal cycle at

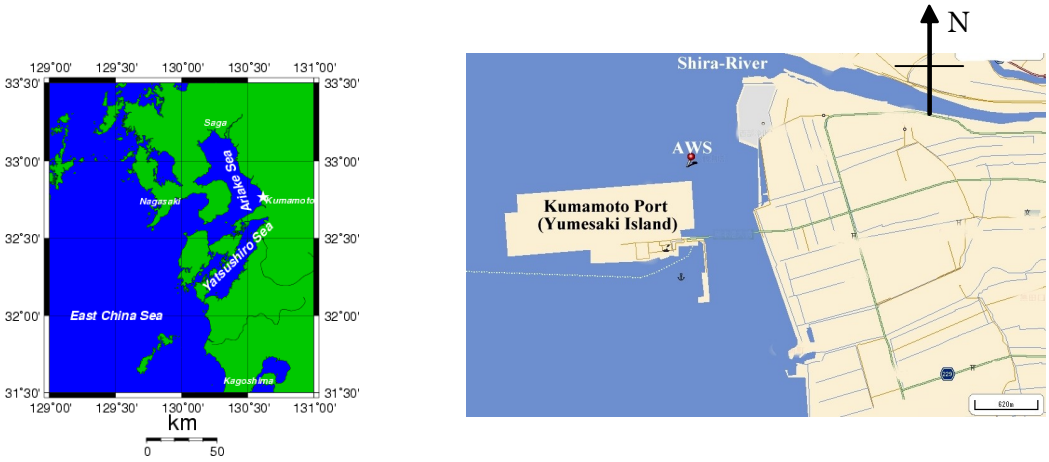

Figure 1. Automated weather station near Kumamoto Port

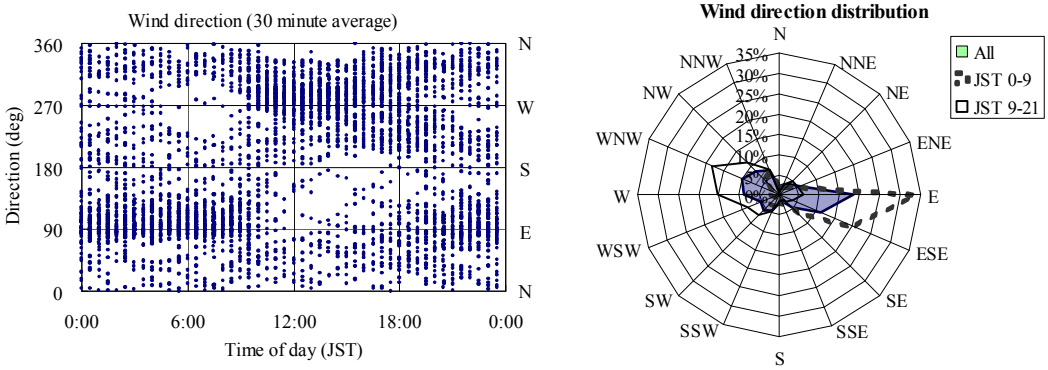

Figure 2. Diurnal distribution of wind direction (clockwise, 0º from North).

the spring tide, but remains submerged at the neap tide. Land and sea breezes are generally

observed on a diurnal cycle (Fig. 2), where the sea breeze (260–320°) is dominant during the day, and the land breeze (~90°) is dominant at night.

Other meteorological variables such as air temperature and relative humidity were also measured by the AWS, as listed in Table 1. A four-component radiation system was installed to observe the surface radiation budget based on measurements of the upward and downward component of shortwave (280–750 nm) and longwave (around 10 μm) radiation flux. The vertical profile of sediment temperature was also measured. All systems except for the turbulent system sampled at 5 s intervals and recorded data as 10 min averages. The data stored by the CR-10X were acquired automatically on a daily basis by telemetry using a mobile phone connected to the logger.

3. Applicability of Monin-Obukhov similarity

Photo 1: Automated Weather Station. (AWS)

Photo 2: Turbulent flux sensors

Table 1. Deployed Sensors

Item	Sensor	Manufacturer	Height (m)	Data logger and collection
Wind Virtual temperature	Sonic anemo-thermometer	81000 (YOUNG)	10.00	CR-5000 (Campbell) with 1G-byte compact flash card
Water vapor CO_2 concentration	H_2O/CO_2 gas analyzer	LI-7500 (Li-Cor)	10.00	
Water temperature Soil temperature	Thermocouple		0.3 -0.01~0.90	
Barometric pressure	Digital Barometer	PTB210 (VAISALA)	6.15	CR-5000 CR-10X
Air temperature Relative humidity	Pt-100 Capacitant Humidity sensor	HMP45A (VAISALA)	7.12	CR-10X (Campbell) Accessed daily by telemetry (dial up via mobile phone)
Precipitation	Tipping Bucket Rain Gauge	TK-1 (Takeda)	6.70	
Four-component radiation	4 component radiometer	MR-40 (EKO)	6.73	
Water Level	Sonic reflectrometer	SR-50 (Campbell)	6.35	

3.1. *Basic theory and stability parameter*

According to the Monin-Obukhov similarity theory (Monin and Obukhov, 1954), any dimensionless characteristic of turbulence is dependent only upon z/L, as given by

$$\frac{z}{L} = \frac{\kappa g z T_*}{T u_*^{\,2}} = -\frac{\kappa g z \overline{w'T'}}{T u_*^{\,3}}, \tag{1}$$

where κ is the von Kármán constant (= 0.40), g is the acceleration of gravity (= 9.8 ms^{-2}), z is the measurement level of the surface, T is the mean air temperature in Kelvin, u_* is the friction velocity, and T_* is the temperature scale. The friction velocity, temperature scale and humidity scale (q_*) are defined

$$\begin{aligned} u_*^{\,2} &= -\left(\overline{u'w'}\right) \\ T_* &= -\left(\overline{w'T'}\right)/u_* \\ q_* &= -\left(\overline{w'q'}\right)/u_* \end{aligned} \tag{2}$$

where overlines denote time averages and primes denote the turbulent fluctuation from the average. The statistical time scale was taken as 30 min (i.e., 18000 samples) in this study.

In the inter-tidal zone, the measurement level from the surface varies according to the water level. In this study, the stability parameter ζ is defined in terms of the mean water level $\bar{\eta}$ as

$$\zeta = \frac{z - \bar{\eta}}{L}, \tag{3}$$

where z (= 10 m) is the measurement level from the sea-bottom surface. For a more exact definition, the aerodynamic surface roughness length z_{0m}, zero plane displacement d due to wave motion, or some factor indicating the trend of the water level should be included in ζ. However, these factors are sufficiently smaller than $z - \bar{\eta}$ to be considered negligible.

3.2 *Data Processing*

To obtain the turbulent statistics value from the sampled wind, temperature and humidity dataset, several correcting and filtering processes are required. The air temperature, measured by the sonic anemo-thermometer, was corrected with respect to the traverse wind and specific humidity q by

$$T_{SV} = T_S(\text{uncor}) + \frac{V_n^{\,2}}{403} \tag{4}$$

$$T = T_{SV}\left(1 - 0.514q\right), \tag{5}$$

where T_{SV} represents the virtual temperature in Kelvin after correction for horizontal wind, T_S(uncor) is the temperature before correction, and V_n is the horizontal wind speed after translating the coordinate system accounting for the axis of the main stream direction.

To eliminate the linear trend in the 30 min data, a linear regression function $f_s(t) = a_s t + b_s$ for the scalar constituent was derived by a linear least-squares method. The time series data s_d after removal of the linear trend was then obtained as

$$s_d = s - (a_s t + b_s), \tag{6}$$

and was used to compute the turbulent statistics value.

3.3 *Results*

Figure 3 shows the frequency distribution of the atmospheric stability parameter ζ. More than 70% of the data fall under the unstable condition ($\zeta < 0$). Over a typical land surface, the stratification becomes stable and ζ takes a positive value. However, the present results indicate that for the inter-tidal zone, nearly 70% of the data are unstable.

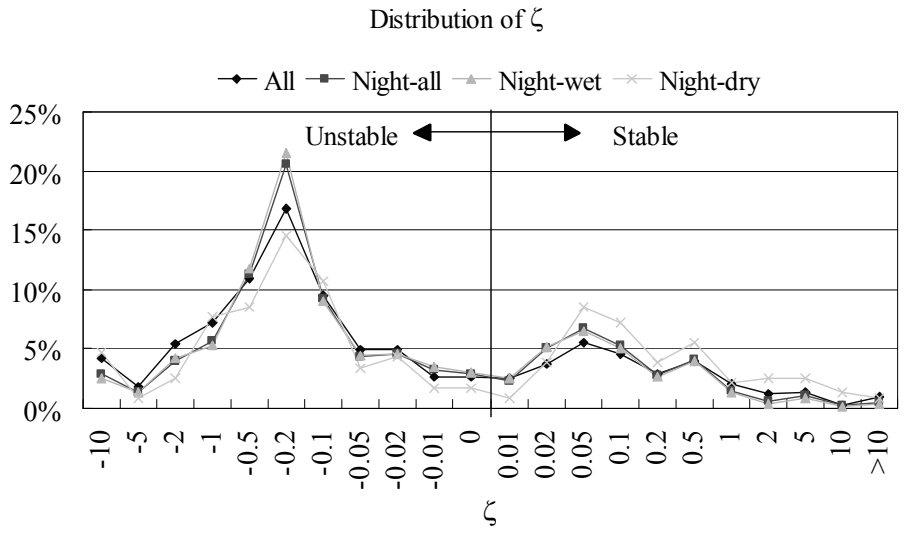

Figure 3. Frequency distribution of stability parameter ζ, where 'All' denotes all data, 'Night-all' denotes data obtained in the period 2000–0600 JST, 'Night-wet' denotes data obtained when the water level was higher than 0.1 m, and 'Night-dry' indicates data obtained when the water level was lower than 0.1 m.

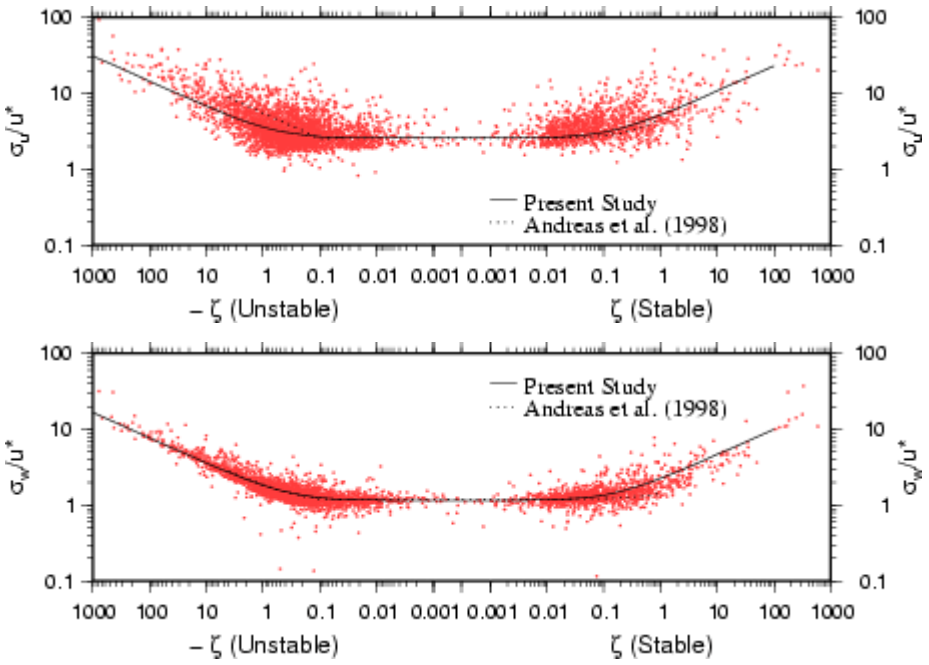

Figure 4. Scatter plot of nondimensional standard deviation of vertical wind (upper) and horizontal wind (lower) versus stability parameter ζ

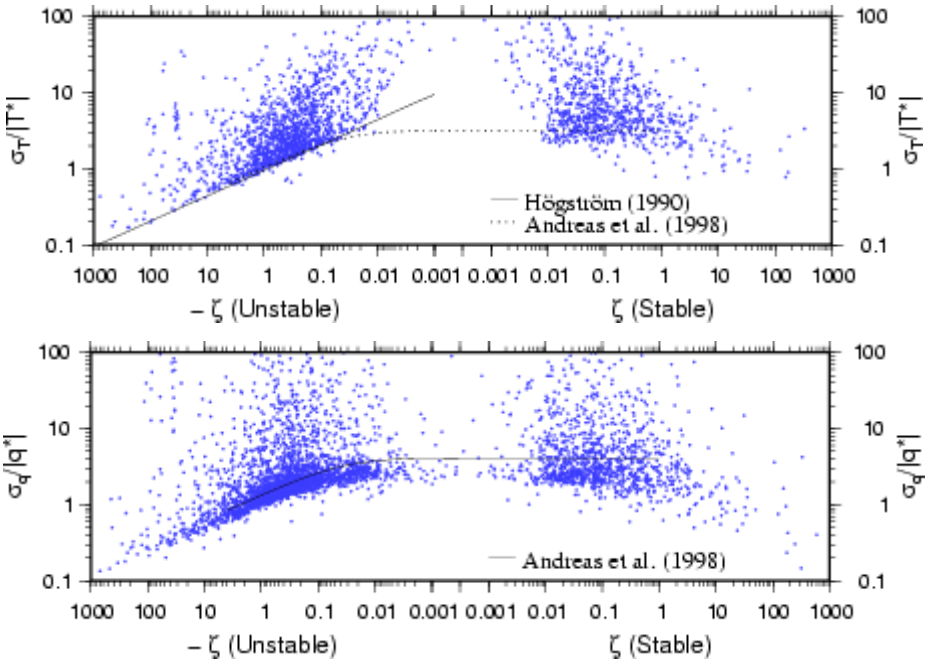

Figure 5. Scatter plot of nondimensional standard deviation of temperature (upper) and specific humidity (lower) versus stability parameter ζ

Figure 4 shows a scatter plot of the nondimensional standard deviation of the horizontal wind (in the main stream direction) and the vertical wind versus the stability parameter ζ. All observed data are plotted in Figure 4. The dotted curve shows the function of Andreas et al. (1998) determined for grassland observation data, as given by

$$\frac{\sigma_u}{u_*} = \begin{cases} 5.49(-\zeta)^{1/3} & (-4 \le \zeta \le -0.1) \\ 2.55 & (-0.1 < \zeta \le 0) \\ 2.55(1+0.8\zeta) & (0 < \zeta \le 1) \end{cases} \tag{7}$$

$$\frac{\sigma_w}{u_*} = \begin{cases} 1.20(0.70 - 3.0\zeta)^{1/3} & (-4 \le \zeta \le -0.1) \\ 1.20 & (-0.1 < \zeta \le 0) \\ 1.20(1+0.2\zeta) & (0 < \zeta \le 1) \end{cases}, \tag{8}$$

Although the plot of σ_u/u_* in the present study appears to have large scatter compared to σ_w/u_*, there is a clear concentration of data points in the vicinity of the average. From this distribution it can be seen that the nondimensional standard deviation of wind component becomes larger as the stability parameter decreases in the unstable regime ($\zeta < -1$) or increases on the stable side ($\zeta > 0.1$). The best-fit functions for σ_u/u_* and σ_w/u_* are defined by

$$\frac{\sigma_u}{u_*} = \begin{cases} 2.55(1-1.8\zeta)^{1/3} & (\zeta \le 0) \\ 2.45(1+7.4\zeta)^{1/3} & (\zeta > 0) \end{cases} \tag{9}$$

$$\frac{\sigma_w}{u_*} = \begin{cases} 1.15(1-3\zeta)^{1/3} & (\zeta \le 0) \\ 1.15(1+6.5\zeta)^{1/3} & (\zeta > 0) \end{cases}, \tag{10}$$

and are shown as solid lines in Figure 4. The nondimensional standard deviation of wind speed appears to obey the Monin-Obukhov similarity, independent of the surface coverage (seawater or sea-bottom surface).

Figure 5 shows the nondimensional standard deviation of temperature and specific humidity for all observed data. Similar to Figure 4, the empirical function for the scalar constituent by Andreas et al. (1998),

$$\frac{\sigma_s}{|s_*|} = \begin{cases} C_1(1-C_2\zeta)^{-1/3} & (\zeta \le 0) \\ C_1 & (\zeta > 0) \end{cases} \tag{11}$$

is plotted as a dotted line in the figure using coefficients of $C_1 = 3.2$ and $C_2 = 28.2$ for temperature and $C_1 = 4.2$ and $C_2 = 28.4$ for specific humidity. The function of Högström (1990) for the unstable condition ($\sigma_T/|T_*| = (-0.95\zeta)^{-1/3}$) is also shown (solid line). The temperature and specific humidity exhibit large scatter in both the stable and unstable conditions, although a decreasing trend can be seen at high instability of stratification. This wide scatter appears to be due to horizontal heterogeneity of the scalar constituent due to surface characteristics in the vicinity of the site.

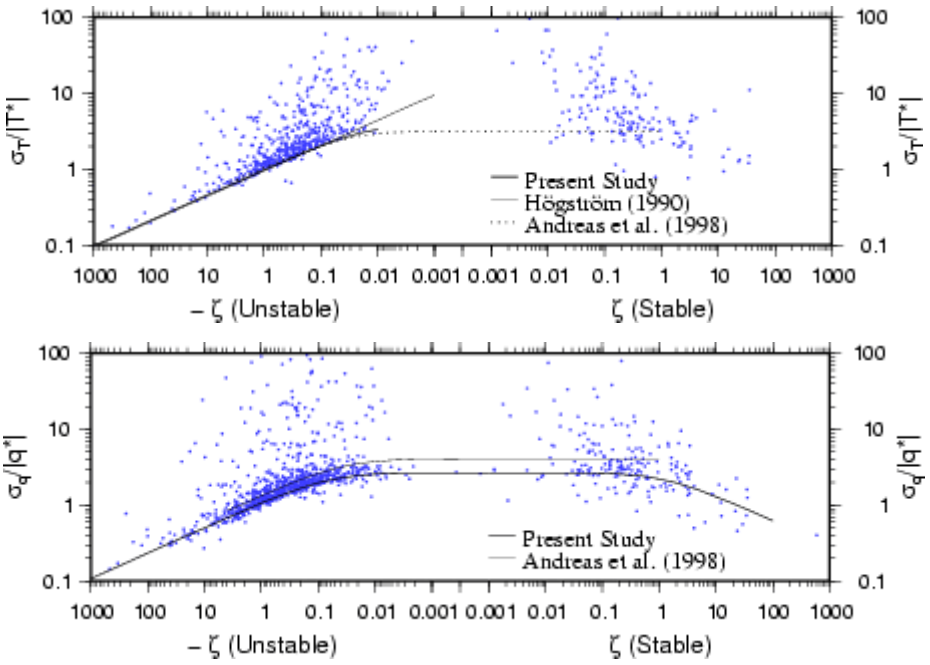

Figure 6. Scatter plot of nondimensional standard deviation of temperature (upper) and specific humidity (lower) versus stability parameter ζ for sea breeze conditions (260–330°)

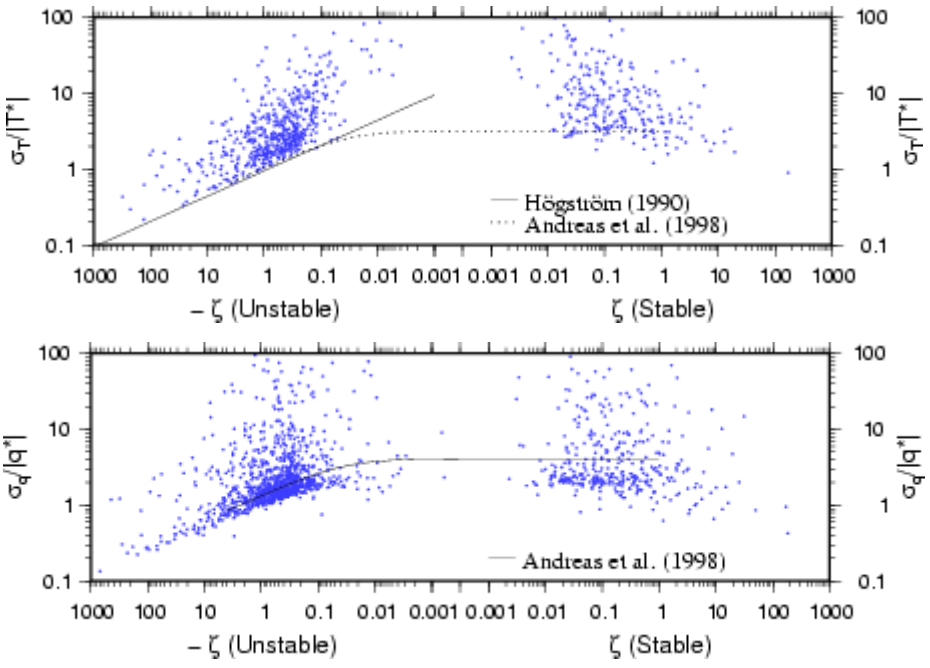

Figure 7. Scatter plot of nondimensional standard deviation of temperature (upper) and specific humidity (lower) versus stability parameter ζ for land breeze conditions (60–130°)

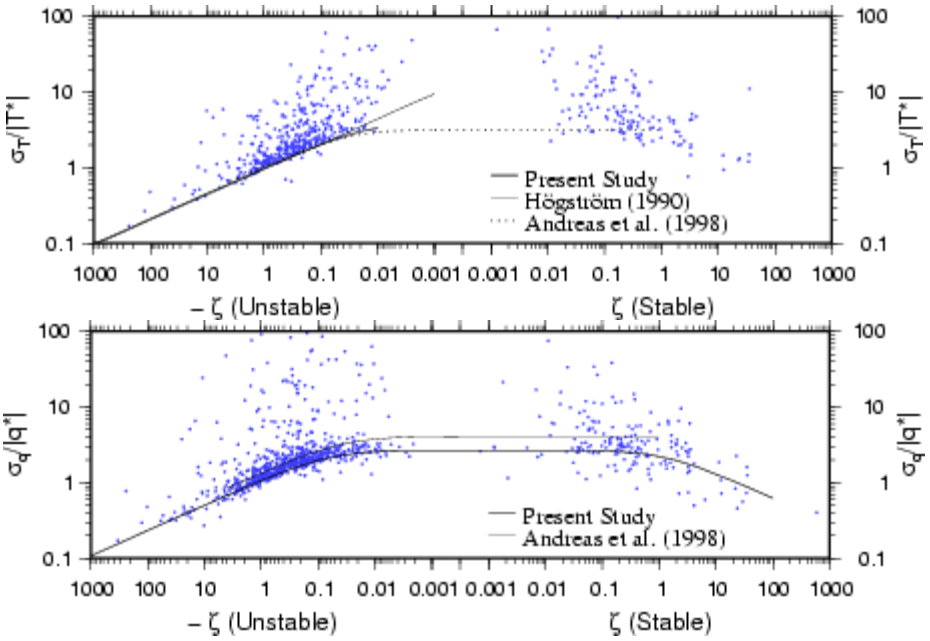

Figure 8. Scatter plot of nondimensional standard deviation of temperature (upper) and specific humidity (lower) versus stability parameter ζ for sea breeze conditions (260–330°) with submerged tidal flat (water depth greater than 0.01 cm)

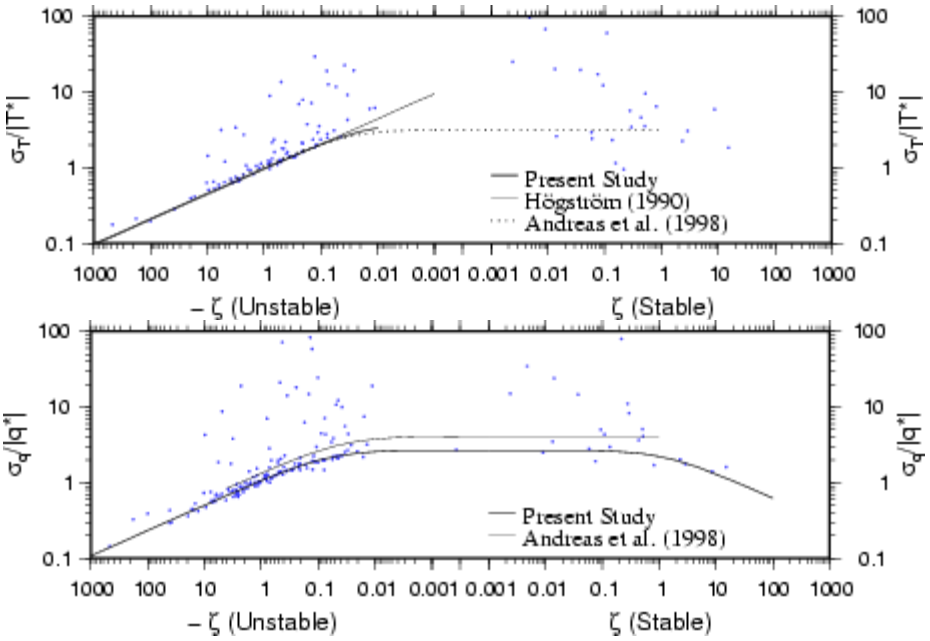

Figure 9. Scatter plot of nondimensional standard deviation of temperature (upper) and specific humidity (lower) versus stability parameter ζ for sea breeze conditions (260–330°) with exposed tidal flat (water depth less than 0.01 cm)

The effect of surface heterogeneity is discussed by classifying the observed data according to the wind direction. The data fall into two major groups; sea breeze conditions (260–330°), and land breeze conditions (60–130°). Figures 6 and 7 show the $\sigma_T/|T_*|$ and $\sigma_q/|q_*|$ data under each of these conditions. Under sea breeze conditions, a –1/3 power functional relationship with ζ can be clearly seen in the unstable regime for both $\sigma_T/|T_*|$ and $\sigma_q/|q_*|$. The most suitable functions for $\sigma_T/|T_*|$ and $\sigma_q/|q_*|$ are given by

$$\frac{\sigma_T}{|T_*|} = 4(1-68\zeta)^{-1/3} \qquad (\zeta \le -0.01) \tag{12}$$

$$\frac{\sigma_q}{|q_*|} = \begin{cases} 2.7(1-15.5\zeta)^{-1/3} & (\zeta \le 0) \\ 2.7(1+0.8\zeta)^{-1/3} & (\zeta > 0) \end{cases} \tag{13}$$

as indicated by the bold line in Figure 5. The neutral condition of $\sigma_q/|q_*|$ in this study (= 2.7) is smaller than that of Andreas et al. (1998) ($C_1 = 4.1$), implying that the correlation $R^2 = (u^*q^*)^2/\sigma_w^2\sigma_q^2$ in the inter-tidal zone under sea breeze conditions is stronger (closer to unity) than over the land surface. On the other hand, the $\sigma_T/|T_*|$ and $\sigma_q/|q_*|$ data under land breeze conditions (Fig. 6) are scattered more widely, and the values tend to be higher than under sea breeze conditions, implying a weaker correlation between w and T, and between w and q.

The surface conditions, whether submerged or exposed, play an important role in the applicability of the similarity theorem. Figures 8 and 9 show plots of $\sigma_T/|T_*|$ and $\sigma_q/|q_*|$ under submerged and exposed conditions under a prevailing sea breeze. In exposed conditions, the functional relationships between $\sigma_T/|T_*|$ and ζ,, and between $\sigma_q/|q_*|$ and ζ, can be more clearly resolved than under submerged conditions.

4. Power spectra

Figures 10 to12 shows the normalized power spectra for w, T and q under various conditions. The normalized spectrum density $f_s(n)$ is defined here as

$$f_s(n) = \frac{nS_s(n)}{\int S_s(n)dn}, \tag{14}$$

where $S_s(n)$ represents the original spectrum density for the property s. In all figures, the normalized power spectrum density decreases in proportion to a –2/3 power of frequency above the turbulent peak frequency n_p (0.01–0.1 Hz)

For daytime sea breeze conditions (314°), as shown in Figure 10, the shapes of the f_w, f_q, and f_T function are very similar, except the low-frequency range ($n < 0.01$ Hz) of f_T. In the case of the land breeze (Figs. 11 and 12), on the other hand, the spectrum densities for temperature and specific humidity in the low-frequency range ($n < 0.01$ Hz) are much higher. The peak frequency for T (~0.1 Hz) shown in Figure 11 is shifted downward compared to that for w or q (~0.4 Hz). In Figures 11 and 12, the lower-frequency range of T and q includes larger scale motion separate from the turbulent motion around the site. From the mean horizontal wind speed of U = 1–5 ms^{-1}

and the time scale of $\Delta\tau$ = 100–1000 s indicated in these two figures, the length scale ΔX is estimated to be $\Delta X = U\Delta\tau$ = 100–5000 m, which is comparable to the distance from the AWS to the island or the mainland (Fig. 1). A discrete variation in temperature or humidity may also be included in this value. The effect of local heterogeneity is discussed below using the turbulent variance equation.

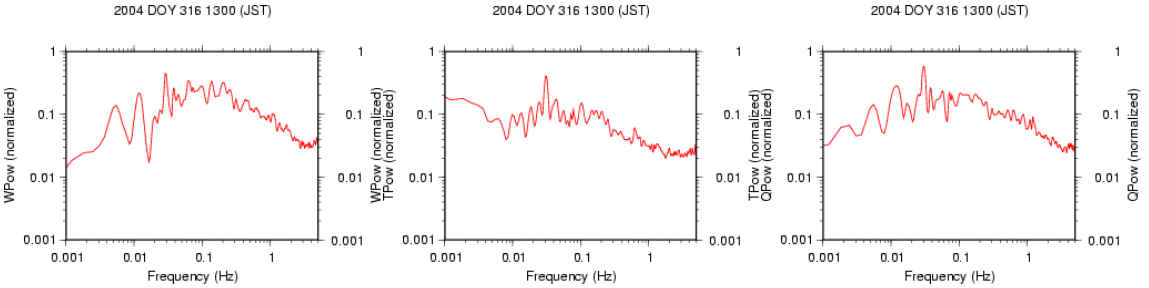

Figure 10. Normalized power spectra of vertical wind speed (left), temperature (center) and specific humidity (right) under free-convective sea breeze conditions (ζ = –1.69; DOY 316; 12 Nov. 2004, 13:00 JST)

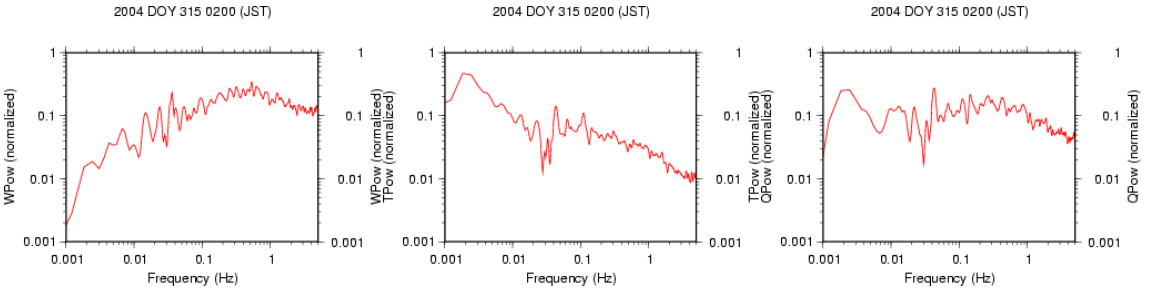

Figure 11. Normalized power spectra of vertical wind speed (left), temperature (center) and specific humidity (right) under stable nighttime land breeze conditions (ζ = 0.026; DOY 315; 11 Nov. 2004, 2:00 JST)

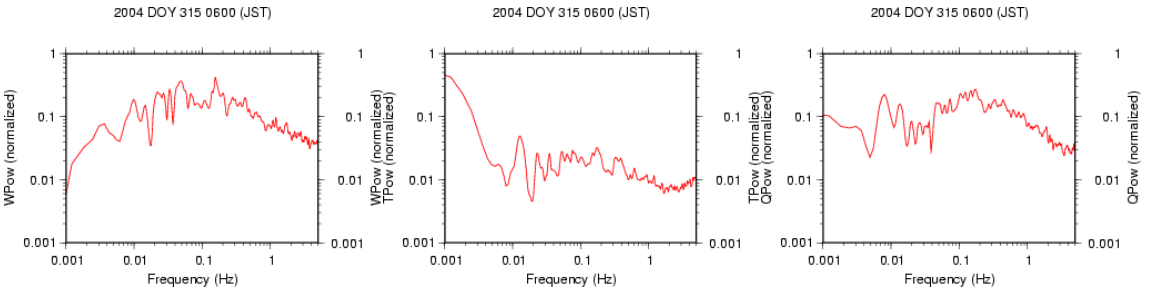

Figure 12. Normalized power spectra of vertical wind speed (left), temperature (center) and specific humidity (right) under unstable land breeze conditions (ζ = –0.027; DOY 315; 11 Nov. 2004, 6:00 JST)

5. Theoretical Discussion

5.1. *Basic Equation of turbulent variance of the scalar constituent*

The equation of temperature variance ($\overline{T'^2}$) and specific humidity variance ($\overline{q'^2}$) can be written as (e.g., Garatt, 1992)

$$\frac{\partial \overline{T'^2}}{\partial t} + \overline{u}_j \frac{\partial \overline{T'^2}}{\partial x_j} = -2\overline{u'_j T'}\frac{\partial \overline{T}}{\partial x_j} - \frac{\partial \overline{T'^2 u'_j}}{\partial x_j} + 2\kappa_T \overline{T'\frac{\partial^2 T'}{\partial x_j^2}} + 2(\rho c_p)^{-1}\overline{T'\frac{\partial R'_j}{\partial x_j}} \tag{15}$$

$$\frac{\partial \overline{q'^2}}{\partial t} + \overline{u}_j \frac{\partial \overline{q'^2}}{\partial x_j} = -2\overline{u'_j q'}\frac{\partial \overline{q}}{\partial x_j} - \frac{\partial \overline{q'^2 u'_j}}{\partial x_j} + 2\kappa_q \overline{q'\frac{\partial^2 q'}{\partial x_j^2}}, \tag{16}$$

where $R'_j = Tu_j - \overline{Tu_j}$ represents the radiative heat flux, and κ_T and κ_q are the molecular thermal and molecular vapor diffusivities. The second terms on the left-hand side of these equations represent the advection of temperature and humidity variance. The first terms on the right-hand side are the production terms resulting from the interaction of turbulence and the mean gradient, while the second terms are momentum terms that can be interpreted as the transport of $\overline{T'^2}$ or $\overline{q'^2}$ by turbulent fluctuations with local loss and gain due to divergence of the turbulent flux. The third terms on the right-hand side represents molecular thermal and humidity diffusion and the fourth term on the right-hand side of Eq. (15) represents radiative transfer, which is negligible and can be ignored.

Under horizontal homogeneous surface condition, Eqs. (15) and (16) can be simplified as

$$\frac{\partial \overline{T'^2}}{\partial t} = -2\overline{w'T'}\frac{\partial \overline{T}}{\partial z} - \frac{\partial \overline{T'^2 w'}}{\partial z} + 2\kappa_T \left(\frac{\partial \overline{T'}}{\partial z}\right)^2 \tag{17}$$

$$\frac{\partial \overline{q'^2}}{\partial t} = -2\overline{w'q'}\frac{\partial \overline{q}}{\partial z} - \frac{\partial \overline{q'^2 w'}}{\partial z} + 2\kappa_q \left(\frac{\partial \overline{q'}}{\partial z}\right)^2. \tag{18}$$

According to Högström (1990), the second term on the right-hand side of Eqs. (17) and (18) is negligible and can be ignored. Hence, in the steady state (i.e., right hand side = 0), production due to the mean vertical temperature or humidity gradient is balanced with destruction due to molecular conditions.

However, in the situation considered in this study, the horizontal gradient of air temperature may become significant when the wind is directed from land or the sediment surface is exposed. To simplify the discussion, the x_1 axis is set parallel to the main stream direction such that $\overline{u_1} \geq 0$ (and $\overline{u_2} = 0$). It is also assumed that homogeneity exists in the x_2 direction, that is, $\partial \overline{s} / \partial x_2 = 0$. Equations (15) and (16) can then be rewritten as

$$\frac{\partial \overline{T'^2}}{\partial t}+\bar{u}\frac{\partial \overline{T'^2}}{\partial x}+\frac{d\bar{h}}{dt}\frac{\partial \overline{T'^2}}{\partial z}=-2\overline{u'T'}\frac{\partial \bar{T}}{\partial x}-2\overline{w'T'}\frac{\partial \bar{T}}{\partial z}-\frac{\partial \overline{T'^2u'}}{\partial x}-\frac{\partial \overline{T'^2w'}}{\partial z}+2\kappa_T\overline{T'\frac{\partial^2 T'}{\partial x^2}}+2\kappa_T\overline{T'\frac{\partial^2 T'}{\partial z^2}} \quad (19)$$

$$\frac{\partial \overline{q'^2}}{\partial t}+\bar{u}\frac{\partial \overline{q'^2}}{\partial x}+\frac{d\bar{h}}{dt}\frac{\partial \overline{q'^2}}{\partial z}=-2\overline{u'q'}\frac{\partial \bar{q}}{\partial x}-2\overline{w'q'}\frac{\partial \bar{q}}{\partial z}-\frac{\partial \overline{q'^2u'}}{\partial x}-\frac{\partial \overline{q'^2w'}}{\partial z}+2\kappa_T\overline{q'\frac{\partial^2 q'}{\partial x^2}}+2\kappa_T\overline{q'\frac{\partial^2 q'}{\partial z^2}}, \quad (20)$$

respectively. The third term on the right-hand side represents transport due to the vertical gradient of temperature or humidity variance with tidal motion, and is applicable when the sediment surface is submerged according to the tide. The water level change rate due to tidal motion is on the order of $d\bar{h}/dt \cong 3.0 \times 10^{-4}$ m s^{-1}, which is sufficiently small compared to the horizontal wind speed (~5 m s^{-1}) to be ignored.

5.2. *Dependency of variance on wind direction*

Under sea breeze conditions, although the sediment surface is exposed in the inter-tidal zone on the tidal cycle, the sediment surface remains wet due to the low evaporation rate (2~4 mm day^{-1}) and the low infiltration rate of soil moisture. The horizontal gradient of specific humidity and its statistics is thus negligible and can be ignored. Equation (20) can therefore be approximated as

$$\frac{\partial \overline{q'^2}}{\partial t}+\frac{d\bar{h}}{dt}\frac{\partial \overline{q'^2}}{\partial z}\approx -2\overline{w'q'}\frac{\partial \bar{q}}{\partial z}-\frac{\partial \overline{q'^2w'}}{\partial z}+2\kappa_T\overline{q'\frac{\partial^2 q'}{\partial z^2}} \quad (21)$$

As the second term on the left-hand side is actually negligible from the above discussion, Eq. (21) reduces to the same form as Eq. (18). Hence, in the case of a sea breeze under near neutral conditions, the characteristics of turbulent humidity in the inter-tidal zone are similar to those over a homogeneous wet surface. During periods of high water level, the horizontal gradient of temperature and its statistics are negligible. Hence, a similar discussion can be applied in that situation. These results indicate that the difference in horizontal temperature gradient and its statistical properties between exposed and submerged tidal flat conditions is relatively unimportant (Fig. 9)

Under a prevailing land breeze, on the other hand, the contrast in mean temperature, humidity, and the corresponding statistics between the inter-tidal zone and land is much more pronounced than that between the inter-tidal zone and offshore. The horizontal gradient terms in Eqs. (19) and (20) are thus expected not to be negligible. That is, the standard deviations of temperature and specific humidity are likely to be affected by the contrast between the land and the inter-tidal zone through horizontal advection (second term on the left-hand side), and through the horizontal gradient of the production term (first term on the right-hand side).

6. Concluding Remarks

The nondimensional standard deviation of wind speed over the inter-tidal zone of the Ariake Sea was found to obey Monin-Obukhov similarity, which is notionally valid only over horizontal homogeneous land surfaces. The nondimensional standard deviation of temperature and specific humidity also obeyed the Monin-Obukhov similarity under conditions of a prevailing sea breeze,

whereas the temperature and specific humidity under land breeze conditions were found to be widely scattered and the relationships with the stability parameter to be less clear. The heterogeneity of temperature and humidity on the windward side was thus found to be the most important factor determining whether the nondimensional standard deviations of the properties can be adequately described by similarity theory.

Acknowledgements

This study was supported by grant for scientific study from Japan Society for the Promotion of Science (A-2-1420872), and by grant-in-aid for young scientists from Ministry of Education Culture, Sports Science and Technology (B-17710016).

References

Andreas, E.L., Hill, J.R., Gosz, J.R., Moore, D.L. Otto, W.D., and Sarma A.D. (1998). Statistics of surface-layer turbulence over terrain with meter-scale heterogeneity, *Boundary-Layer, Meteor*., **86**, 379-408.

Garatt, J.R. (1992) *The Atmospheric Boundary Layer*, Cambridge University Press.

Högström, U. (1990). Analysis of turbulence structure in the surface layer with a modified similarity formulation for near neutral conditions, *J. Atmos. Sci.* **49**, 1949-72.

Kadar, B.A. and Yaglom A.M. (1989). Mean fields and fluctuation moments in unstably stratified turbulent boundary layers*, J. Fruid Mech*., **212**, 637-662.

Kruit, R.J.W., Holtslag, A.A.M., and Tijm, A.B.C (2004). Scaling of the sea-breeze strength with observations in the neatherlands, *Boundary-Layer Meteor.*, **112**, 369-380.

Lange, B., Larsen, S., Højstrup, J., and Barthelmie, R., (2004). The influence of thermal effects on the wind speed profile of the coastal marine boundary layer. *Boundary-Layer Meteor.,* **112**, 587-617.

Monin, A. S. and Obukhov A. M. (1954). Basic laws of turbulent mixing in the atmosphere near the ground, *Tr. Akad. Nauk SSSR Geofiz. Inst*. **24**(151), 163-87.

Plant, R.S., and Atkinson B.W. (2002). Sea-breeze modification of the growth of a marine internal boundary layer. *Boundary-Layer Meteor.*,**104**, 201-228.

.